

CONSTRAINING THE LYMAN ALPHA ESCAPE FRACTION WITH FAR-INFRARED OBSERVATIONS OF LYMAN ALPHA EMITTERS

JULIE L. WARDLOW^{1,2†}, S. MALHOTRA³, Z. ZHENG³, S. FINKELSTEIN⁴, J. BOCK^{5,6}, C. BRIDGE⁵, J. CALANOG¹, R. CIARDULLO^{7,8}, A. CONLEY⁹, A. COORAY^{1,5}, D. FARRAH¹⁰, E. GAWISER¹¹, C. GRONWALL^{7,8}, S. HEINIS¹², E. IBAR^{13,14}, R.J. IVISON¹⁵, G. MARSDEN¹⁶, S.J. OLIVER¹⁷, J. RHOADS³, D. RIECHERS¹⁸, B. SCHULZ^{5,19}, A.J. SMITH¹⁷, M. VIERO⁵, L. WANG²⁰, M. ZEMCOV^{5,6}

Draft version September 25, 2018

ABSTRACT

We study the far-infrared properties of 498 Lyman Alpha Emitters (LAEs) at $z = 2.8, 3.1$ and 4.5 in the Extended *Chandra* Deep Field-South, using 250, 350 and $500\mu\text{m}$ data from the *Herschel*[‡] Multi-tiered Extragalactic Survey (HerMES) and $870\mu\text{m}$ data from the LABOCA ECDFS Submillimeter Survey (LESS). None of the 126, 280 or 92 LAEs at $z = 2.8, 3.1$ and 4.5 , respectively, are individually detected in the far-infrared data. We use stacking to probe the average emission to deeper flux limits, reaching 1σ depths of ~ 0.1 to 0.4 mJy . The LAEs are also undetected at $\geq 3\sigma$ in the stacks, although a 2.5σ signal is observed at $870\mu\text{m}$ for the $z = 2.8$ sources. We consider a wide range of far-infrared spectral energy distributions (SEDs), including a M82 and an Sd galaxy template, to determine upper limits on the far-infrared luminosities and far-infrared-derived star-formation rates of the LAEs. These star-formation rates are then combined with those inferred from the Ly α and UV emission to determine lower limits on the LAEs Ly α escape fraction ($f_{\text{esc}}(\text{Ly}\alpha)$). For the Sd SED template, the inferred LAEs $f_{\text{esc}}(\text{Ly}\alpha)$ are $\gtrsim 30\%$ (1σ) at $z = 2.8, 3.1$ and 4.5 , which are all significantly higher than the global $f_{\text{esc}}(\text{Ly}\alpha)$ at these redshifts. Thus, if the LAEs $f_{\text{esc}}(\text{Ly}\alpha)$ follows the global evolution then they have warmer far-infrared SEDs than the Sd galaxy template. The average and M82 SEDs produce lower limits on the LAE $f_{\text{esc}}(\text{Ly}\alpha)$ of $\sim 10\text{--}20\%$ (1σ), all of which are slightly higher than the global evolution of $f_{\text{esc}}(\text{Ly}\alpha)$, but consistent with it at the $2\text{--}3\sigma$ level.

Subject headings: galaxies: star formation — galaxies: high-redshift — submillimeter: general

1. INTRODUCTION

The 1216 \AA Ly α emission line is a tracer of the ionizing photons radiated by young stars. The spectral line originates from the $n = 2 \rightarrow 1$ transition of hydrogen and can contain up to $\sim 6\%$ of the bolometric luminosity of a star-forming galaxy (Partridge & Peebles 1967). It reliably identifies star-forming galaxies at redshifts $z > 2$, with Ly α line searches now well-established as a robust method for selecting samples of high-redshift galaxies, both using narrowband images (e.g. Cowie & Hu 1998; Rhoads et al. 2000, 2003; Gronwall et al. 2007; Gawiser et al. 2007; Ouchi et al. 2008; Finkelstein et al. 2008, 2009d; Guaita et al. 2010) and spectroscopic surveys (e.g. Steidel et al. 1999; Deharveng et al. 2008; Blanc et al. 2011). Thousands of photometrically-selected Ly α emitters (LAEs) have been identified, hundreds of which have been spectroscopically confirmed (e.g. Hu et al. 2004; Dawson et al. 2007; Wang et al. 2009) at $z \approx 0.3$ (Deharveng et al. 2008; Finkelstein et al. 2009a; Cowie et al. 2010) to $z \approx 7$ (Iye et al. 2006; Ouchi et al. 2009, 2010; Rhoads et al. 2012; Shibuya et al. 2012).

However, the interpretation of Ly α observations is challenging because Ly α photons interact with the neu-

¹⁹ Infrared Processing and Analysis Center, MS 100-22, California Institute of Technology, JPL, Pasadena, CA 91125

²⁰ Institute for Computational Cosmology, Durham University, South Road, Durham DH1 3LE, UK

[‡] *Herschel* is an ESA space observatory with science instruments provided by European-led Principal Investigator consortia and with important participation from NASA.

[†] jwardlow@dark-cosmology.dk

¹ Department of Physics & Astronomy, University of California, Irvine, CA 92697

² Dark Cosmology Centre, Niels Bohr Institute, University of Copenhagen, Denmark

³ School of Earth and Space Exploration, Arizona State University, Tempe, AZ 85287

⁴ The University of Texas at Austin, Austin, TX 78712

⁵ California Institute of Technology, 1200 E. California Blvd., Pasadena, CA 91125

⁶ Jet Propulsion Laboratory, 4800 Oak Grove Drive, Pasadena, CA 91109

⁷ Department of Astronomy and Astrophysics, Pennsylvania State University, University Park, PA 16802

⁸ Institute for Gravitation and the Cosmos, The Pennsylvania State University, University Park, PA 16802

⁹ Center for Astrophysics and Space Astronomy 389-UCB, University of Colorado, Boulder, CO 80309

¹⁰ Department of Physics, Virginia Tech, Blacksburg, VA 24061

¹¹ Department of Physics and Astronomy, Rutgers, The State University of New Jersey, 136 Frelinghuysen Rd, Piscataway, NJ 08854

¹² Department of Astronomy, University of Maryland, College Park, MD 20742

¹³ UK Astronomy Technology Centre, Royal Observatory, Blackford Hill, Edinburgh EH9 3HJ, UK

¹⁴ Universidad Católica de Chile, Departamento de Astronomía y Astrofísica, Vicuña Mackenna 4860, Casilla 306, Santiago 22, Chile

¹⁵ Institute for Astronomy, University of Edinburgh, Royal Observatory, Blackford Hill, Edinburgh EH9 3HJ, UK

¹⁶ Department of Physics & Astronomy, University of British Columbia, 6224 Agricultural Road, Vancouver, BC V6T 1Z1, Canada

¹⁷ Astronomy Centre, Dept. of Physics & Astronomy, University of Sussex, Brighton BN1 9QH, UK

¹⁸ Department of Astronomy, Space Science Building, Cornell University, Ithaca, NY, 14853-6801

tral hydrogen in the inter-stellar medium (ISM) and are resonantly scattered. Furthermore, due to their short wavelength they are also susceptible to absorption by dust, which further complicates analyses (Neufeld 1991; Hansen & Oh 2006; Finkelstein et al. 2009c). Radiative transfer in the dusty, multiphase and dynamic interstellar medium (ISM) is complex and thus observations of the escape fraction of Ly α photons ($f_{\text{esc}}(\text{Ly}\alpha)$), defined as the ratio of observed to intrinsic Ly α emission, are also useful for probing the clumpiness and distribution of dust and gas in the ISM, which is typically spatially unresolved at high redshift.

Various methods have been applied to estimate the intrinsic Ly α emission, which is required for calculating $f_{\text{esc}}(\text{Ly}\alpha)$. For example, under the case B recombination theory (Baker & Menzel 1938), the intrinsic Ly α line flux can be estimated using the H α line flux, corrected for dust extinction; but measuring both the Ly α and H α lines is possible only over narrow redshift ranges (e.g. Atek et al. 2009; Finkelstein et al. 2011b for $z \sim 0.3$ LAEs, and Hayes et al. 2010; Finkelstein et al. 2011c for $z \sim 2.3$ LAEs). Other methods of estimating the intrinsic Ly α flux rely on Ly α photons ability to trace young stars. Thus, intrinsic Ly α emission is connected to the intrinsic star-formation rate (SFR), which can be estimated from the UV continuum (subject to dust extinction), or X-ray emission (Zheng et al. 2012) which is extinction free, but relies on an empirically calibrated relation between X-ray emission and SFR (Nandra et al. 2002; Grimm et al. 2003; Ranalli et al. 2003; Persic et al. 2004; Symeonidis et al. 2011).

Alternatively, the SFR can be estimated from measurements of the far-infrared continuum emission, which in young galaxies, is emitted by dust heated by young stars (e.g Kennicutt 1998; Egami et al. 2004; Choi et al. 2006; Rieke et al. 2009; Calzetti et al. 2010; Murphy et al. 2011). The Ly α and far-infrared measurements provide complementary views of the non-dusty and dusty regions of a galaxy, respectively. In this paper we use continuum 250, 350, 500 and 870 μm observations to probe the dust emission of three samples of LAEs at $z = 2.8$ (Zheng et al. in prep.), 3.1 (Gronwall et al. 2007; Ciardullo et al. 2012) and 4.5 (Finkelstein et al. 2009d; Zheng et al. 2013). As the LAEs are too faint to be individually detected in the far-infrared data we use a stacking analysis to reach deeper flux limits and investigate the average emission from the sources (c.f. Davies et al. 2013 stacking of $z \sim 4.5$ LAEs at 870 μm). Then, by comparing the integrated SFR derived from the far-infrared luminosity with the integrated SFR derived from the *apparent* Ly α and rest-frame ultra-violet (UV) luminosities the Ly α escape fraction is calculated.

In Section 2 we present the Ly α samples and the far-infrared data used in the analysis. The stacking procedure is described in Section 3 and the far-infrared SEDs of LAEs and the Ly α escape fraction are presented and discussed in Section 4. Our conclusions are presented in Section 5. Throughout this paper we use ΛCDM cosmology with $\Omega_{\text{M}} = 0.27$, $\Omega_{\Lambda} = 0.73$ and $H_0 = 71 \text{ km s}^{-1} \text{ Mpc}^{-1}$.

2. DATA

Ly α emission is easily absorbed by dust, and therefore, LAE selections may preferentially bias against galaxies

with bright far-infrared (dust) emission, although this supposition depends on the distribution of dust in the ISM. Indeed, we note the large fraction of Ly α detections amongst SMGs (e.g. Chapman et al. 2005) and their occasional association with Ly α blobs (Iverson et al. 1998). Measurements of dust absorption from the UV spectral slopes of LAEs also suggest that LAEs will be faint at far-infrared wavelengths (Finkelstein et al. 2009c). Therefore, in this paper we consider LAEs in the Extended *Chandra* Deep Field South (ECDFS) survey region, where extensive deep far-infrared data are available.

2.1. Sample selection

We examine a total of 498 LAEs in the ECDFS in three redshift bins: $z = 2.8$, $z = 3.1$ and $z = 4.5$.

The $z = 2.8$ sample consists of 126 photometrically-selected LAEs identified in narrowband NB466, NB470, and NB475 (all with FWHM $\sim 50\text{\AA}$), with VLT/VIMOS *U*-band (Nonino et al. 2009) and MUSYC *B*-band (Gawiser et al. 2006) coverage. The selection criteria are $U - B \geq 0.8$, $\text{NB} \geq 5\sigma$, and $B - \text{NB} \geq 1$ (Zheng et al. in prep.).

At $z = 3.1$ we examine the 252 and 188 LAEs presented in Gronwall et al. (2007) and Ciardullo et al. (2012), respectively. The samples are photometrically selected using narrowband imaging with slightly different filters (for a comparison see Ciardullo et al. 2012). There is some overlap between the two catalogs; we remove duplicates using a matching radius of $1''$, which results in a final sample of 280 unique $z = 3.1$ LAEs, of which ~ 70 have so far been spectroscopically confirmed.

For the highest redshift sample, at $z = 4.5$, we consider LAEs that were identified in narrowband imaging by Finkelstein et al. (2009d). We consider the 92 of these LAEs that were confirmed with spectroscopic followup observations (46 LAEs; Zheng et al. 2013) or that have not been spectroscopically targeted (44 LAEs). Our conclusions do not change if we only consider the 46 spectroscopically confirmed $z = 4.5$ LAEs, although, due to the larger sample size, the stacked flux and SFR limits are deeper when the photometric LAEs are included.

2.2. Far-infrared data

In the far-infrared we consider deep 250-, 350-, 500- and 870- μm continuum imaging. The 870- μm data are from the LABOCA ECDFS Submillimeter Survey (LESS; Weiß et al. 2009) and the 250-, 350- and 500- μm data were taken with SPIRE (Griffin et al. 2010) on the *Herschel Space Observatory* (Pilbratt et al. 2010) as part of the *Herschel* Multi-Tiered Extragalactic Survey²³ (HerMES; Oliver et al. 2012).

The LESS 870- μm maps and catalogs are presented in Weiß et al. (2009). The data cover $30' \times 30'$, including all target LAEs, to a roughly uniform depth of $\sigma \sim 1.2 \text{ mJy beam}^{-1}$. These data were taken with the LABOCA instrument on the 12m APEX telescope resulting in a $19''$ beam (FWHM). The catalog contains 126 sources down to 3.7σ , corresponding to $\sim 4.4 \text{ mJy beam}^{-1}$.

The HerMES 250, 350 and 500 μm data in the ECDFS are nested, with coverage extending over a $204' \times 170'$

²³ <http://hermes.sussex.ac.uk>

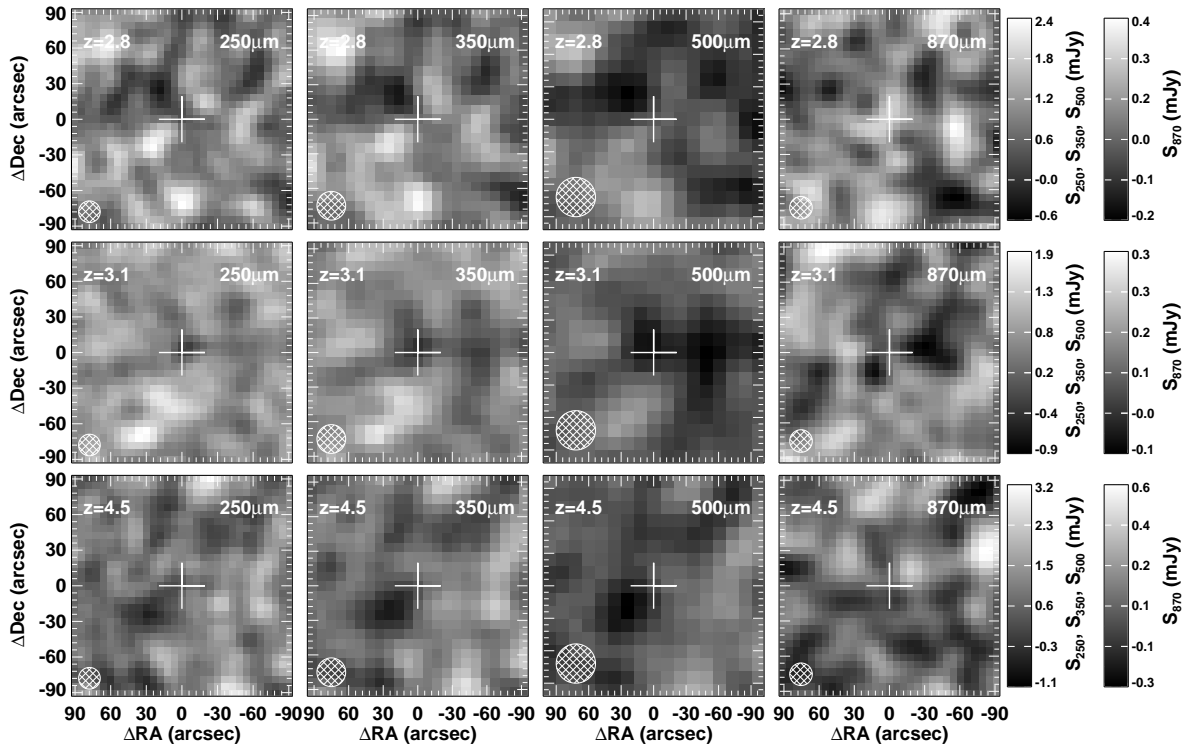


Figure 1. $180 \times 180''$ cutouts of the $z = 2.8, 3.1$ and 4.5 (top to bottom) stacked LAEs at $250, 350, 500$ and $870 \mu\text{m}$ (left to right). The LAEs are positioned at the centers of the stacks – marked with crosses – and are not detected at $\geq 3\sigma$ in any of the far-infrared data. The shaded circles show the size of the beam at each wavelength.

area. All the target LAEs are located in the central $30' \times 30'$ of these data. The central $20' \times 20'$ region (enclosing $\sim 35\%$ of the LAEs) has the deepest data, reaching down to $\sigma \sim 0.9, 0.8$ and $1.1 \text{ mJy beam}^{-1}$ at $250, 350$ and $500 \mu\text{m}$, respectively (excluding confusion; Oliver et al. 2012). The remainder of the central $30' \times 30'$ reaches $\sigma \sim 1.6, 1.3$ and $1.9 \text{ mJy beam}^{-1}$ at $250, 350$ and $500 \mu\text{m}$ (Oliver et al. 2012). For our analyses all the nested datasets are included and thus the maps and catalogs have non-uniform coverage. The *Herschel* beam is $18, 25$ and $36''$ (FWHM) at $250, 350$ and $500 \mu\text{m}$, respectively. Details of the data reduction and map and catalog production are available in Levenson et al. (2010), Viero et al. (2013a), Smith et al. (2012) and Wang et al. (in prep.).

3. ANALYSIS

We begin by cross-matching the LAEs with the HerMES and LESS catalogs to determine whether any are individually detected in the far-infrared. The positional uncertainty of the LAEs is typically $\ll 1''$, which is significantly smaller than that of the far-infrared catalogs due to the large beamsizes of single dish submillimeter telescopes. Therefore, the LAE positional uncertainty can be disregarded when choosing the cross-matching radius and when stacking the far-infrared data (§ 3.1).

For the $19''$ LESS $870\text{-}\mu\text{m}$ beam the 1σ positional uncertainty on the cataloged sources is $\sim 1\text{--}3''$ (Biggs et al. 2011; Hodge et al. 2013), depending on the signal-to-noise ratio (SNR; see Ivison et al. 2007). For cross-matching the LAEs and the LESS sources we choose a liberal search radius of $9''$ – corresponding to $\sim 3\sigma_{\text{pos}}$ for

the most uncertain positions. Three of the LAEs – two at $z = 2.8$ and one at $z = 3.1$ – are positionally matched to a source in the LESS catalog, with separations of 6.5 to $8.3''$. None of the $z = 4.5$ LAEs are matched in the LESS catalog within the $9''$ radius.

Assuming that the 498 LAEs and 126 LESS sources are randomly distributed in the $30 \times 30'$ area we expect to find $\sim 1\text{--}2$ chance superpositions of LAEs and LESS sources, which is consistent with all three of LAE—LESS pairs being chance associations. This interpretation is supported by high-resolution $870 \mu\text{m}$ ALMA continuum observations of the $870 \mu\text{m}$ LABOCA sources (Hodge et al. 2013), which in two of the cases pinpoints non-LAEs as the source of the $870 \mu\text{m}$ emission. In the third case, no $870 \mu\text{m}$ sources are detected in the ALMA observations ($\sigma = 0.33 \text{ mJy beam}^{-1}$; Hodge et al. 2013), which may be the result of blending of several faint far-infrared sources in the LABOCA beam. In this case the association between the LAE and the LABOCA source is either a chance superposition, or the LAE does contribute to the LABOCA source but only a fraction of the detected $870 \mu\text{m}$ flux can be from this galaxy. We conclude that none of the LAEs are robustly individually detected at $870 \mu\text{m}$.

The $250, 350$ and $500 \mu\text{m}$ HerMES catalog is created by blindly extracting sources at $250 \mu\text{m}$, where the beam is smallest ($18''$ FWHM), using those source positions as priors for the longer wavelength data and then identifying any additional 350 and $500 \mu\text{m}$ sources in the residual maps. Therefore, the positional error in the HerMES catalogues is dominated by the $18''$ beam at $250 \mu\text{m}$. The positional error is also typically $\sim 1\text{--}3''$, depending on

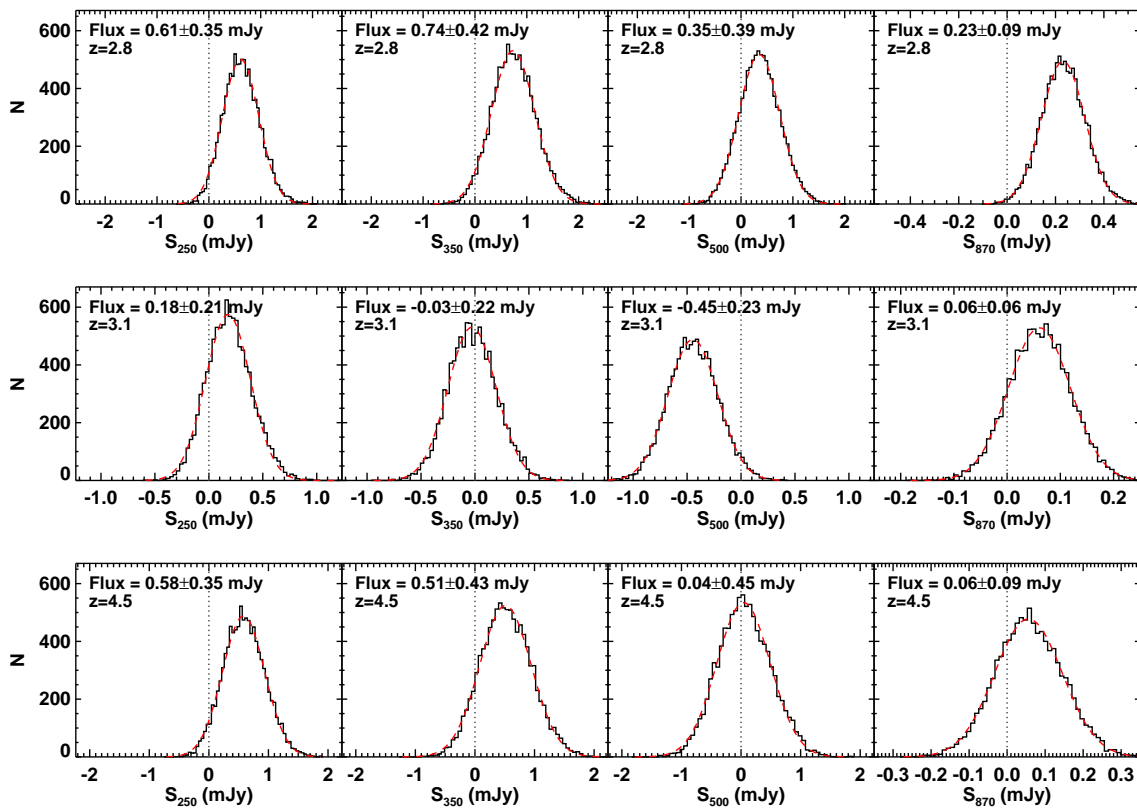


Figure 2. Histograms of the 250, 350, 500 and 870 μm (left to right) stacked flux densities measured in 10,000 bootstrap trials of $z = 2.8$, 3.1 and 4.5 (top to bottom) LAEs. Dashed lines show Gaussian fits to the histograms from which we measure the stack flux densities and detection limits (1σ), written at the top of each panel. None of the LAEs are significantly ($\geq 3\sigma$) detected in any of the data, although at 2.6σ the 870 μm stack of the $z = 2.8$ LAEs approaches this threshold.

the SNR. Therefore, we use the same liberal $9''$ search radius when cross-matching the LAEs with the HerMES catalog. We only consider cataloged sources that are detected at $\geq 3\sigma_{\text{total}}$, where σ_{total} includes confusion noise, in at least one of the three HerMES bands. Within the $9''$ search radius there are two, one and two matches to the $z = 2.8$, 3.1 and 4.5 LAEs, respectively. The five LAE to HerMES positional matches have separations of 3.4 to $7.9''$. Within the $9''$ search radius 4–5 chance superpositions between the ~ 450 HerMES sources and the 498 LAEs are expected – which is consistent with the observed matching rate. Therefore, it is unlikely that any of the matches between the LAEs and 250, 350 and 500 μm catalog are physical associations between the LAEs and the far-infrared flux.

3.1. Stacking

We next stack the far-infrared data at the position of the LAEs, to explore their average emission at 250, 350, 500 and 870 μm . Stacking probes below the nominal detection limit by reducing the background noise so that a measure of the average flux density of the stacked sample can be made (e.g. Peacock et al. 2000; Serjeant et al. 2004; Marsden et al. 2009; Pascale et al. 2009; Ivison et al. 2010; Béthermin et al. 2010; Viero et al. 2012, 2013b; Heinis et al. 2013; Calanog et al. 2013). For a sample of N sources, and in the absence of clustering, stacking decreases the background noise by a factor of \sqrt{N} .

We include all the LAEs in the stacks because none are definitively individually detected, although our conclusions do not change if LAEs with far-IR sources within $9''$ are excluded.

We use the public IDL code²⁴ from Béthermin et al. (2010) to perform separate 250, 350, 500 and 870 μm stacks. In each case a weighted mean stack is performed, with the weighting equal to the inverse of the error map, which accounts for the non-uniform depth of the data. Prior to stacking the maps are resampled to properly centroid on each of the LAEs, and we calibrate them so that the median background level is zero. This increases the flux levels by 1.22, 1.28 and 0.93 mJy at 250, 350 and 500 μm , respectively, and decreases the 870 μm fluxes by 0.04 mJy. Figure 1 shows $180 \times 180''$ regions of the stacked maps.

To robustly measure the flux density and associated detection limit in the stacked maps, we perform bootstrapping with replacement, repeating each stack 10,000 times with a random sampling of the LAEs each time. The stacked flux density in each realization is extracted from PSF fitting to the centers of the stacks. Figure 2 shows histograms of these flux density values for the each of the 10,000 bootstrap samples. Each histogram is fitted with a gaussian and the stacked flux density and 1σ detection limit are determined from the center and standard deviation of the gaussian fit, respectively, as shown

²⁴ Available from www.ias.u-psud.fr/irgalaxies/downloads.php

Table 1
Summary of the stacking results

Waveband (μm)	Flux density ^a (mJy)	Noise ^b (mJy)	$1\sigma^{\Upsilon}$ L _{IR} ($10^{11}L_{\odot}$)				$1\sigma^{\Upsilon}$ SFR ($M_{\odot}\text{yr}^{-1}$)				$1\sigma^{\Lambda}$ $f_{\text{esc}}(\text{Ly}\alpha)$			
			Sd ^c	M82 ^c	Mean ^d	All ^e	Sd ^f	M82 ^f	Mean ^g	All ^h	Sd ⁱ	M82 ⁱ	Mean ^j	All ^k
$z = 2.8$; 126 LAEs														
250	0.61	0.35	1.7	1.3	1.4	1 – 2.1	29	22	24	18 – 36	0.07	0.09	0.08	0.06 – 0.11
350	0.74	0.42	0.94	1.5	1.2	0.9 – 1.8	16	26	20	15 – 30	0.11	0.08	0.10	0.07 – 0.12
500	0.35	0.39	0.64	2	1.3	0.62 – 3	11	34	22	11 – 51	0.15	0.06	0.09	0.04 – 0.15
870	0.23	0.09	0.22	1.3	0.84	0.18 – 2.5	4	23	15	3 – 43	0.26	0.09	0.12	0.05 – 0.28
$z = 3.1$; 280 LAEs														
250	0.18	0.21	1.5	0.93	1.1	0.74 – 1.7	25	16	19	13 – 30	0.06	0.08	0.07	0.05 – 0.10
350	-0.03	0.22	0.68	0.94	0.78	0.59 – 1	12	16	13	10 – 18	0.11	0.08	0.10	0.08 – 0.12
500	-0.45	0.23	0.45	1.3	0.83	0.43 – 1.8	8	22	14	7 – 30	0.15	0.06	0.09	0.05 – 0.16
870	0.06	0.06	0.15	0.86	0.54	0.13 – 1.6	3	15	9	2 – 27	0.33	0.09	0.13	0.05 – 0.37
$z = 4.5$; 92 LAEs														
250	0.58	0.35	11	4.3	6.1	3.1 – 13	187	75	104	53 – 229	0.03	0.08	0.06	0.03 – 0.10
350	0.51	0.43	4.8	3.4	3.9	2.7 – 6	83	59	67	47 – 103	0.07	0.09	0.08	0.06 – 0.11
500	0.04	0.45	2.2	3.5	2.7	2.1 – 4	38	61	47	36 – 69	0.13	0.09	0.11	0.08 – 0.13
870	0.06	0.09	0.32	1.3	0.82	0.3 – 2.1	6	22	14	5 – 37	0.31	0.18	0.23	0.13 – 0.32

Note. — Υ Upper limits. Λ Lower limits.

^a Observed flux density in the stack; all are insignificant ($< 3\sigma$; Section 3.1). ^b 1σ noise (Section 3.1). ^c 1σ upper limit on the 8–1000 μm far-infrared luminosity calculated assuming the Sd or M82 SED (Section 4.1). ^d Mean 1σ upper limit on the 8–1000 μm far-infrared luminosity of all of the SEDs shown in Fig. 3 (Section 4.1). ^e 1σ range of upper limits on the 8–1000 μm far-infrared luminosity from all of the SEDs shown in Fig. 3 (Section 4.1). ^f 1σ upper limit on the star-formation rate calculated from the far-infrared luminosity from the Sd or M82 SED using Kennicutt (1998). ^g Mean 1σ upper limit on the star-formation rate of all of the SEDs shown in Fig. 3 and calculated from the far-infrared luminosity using Kennicutt (1998). ^h 1σ range of upper limits on the star-formation rate from the range of far-infrared luminosities from all of the SEDs shown in Fig. 3. ⁱ 1σ lower limit on the Ly α escape fraction for the SFR derived from the Sd or M82 SED (Section 4.2). ^j 1σ lower limit on the Ly α escape fraction for the mean SFR of all the SEDs (Section 4.2). ^k Range of 1σ lower limits on the Ly α escape fraction for the SFRs of all the SEDs (Section 4.2).

on Figure 2 and listed in Table 1.

The average flux densities of the LAEs measured from stacking are presented in Table 1. None of the LAEs are detected at $\geq 3\sigma$ in any of the far-infrared data. The most significant flux is from the $z = 2.8$ LAEs, which are observed at 2.6σ in the $870\mu\text{m}$ stack. All the other stacks are $< 2\sigma$. The detection limits presented are measured using the method above and are consistent with the pixel-to-pixel variance in the stacked images (Figure 1). For the $z = 4.5$ LAEs the $870\mu\text{m}$ limit is also consistent with the result from Davies et al. (2013) who recently stacked the same LAEs on a source-subtracted LESS map and also found a non-detection.

The measured flux densities from stacking low-resolution data, such as those considered here, can be boosted by clustering, due to multiple sources occupying the far-infrared beam (e.g. Fernandez-Conde et al. 2010; Serjeant et al. 2008, 2010; Béthermin et al. 2010; Greve et al. 2010; Kurczynski & Gawiser 2010; Penner et al. 2011; Viero et al. 2013b). Accounting for such an effect would decrease the limits quoted above, and therefore, we disregard this effect as we have only constrained upper limits on the flux densities. Furthermore, we note that LAEs are only weakly clustered (e.g. Ouchi et al. 2010), with $r_0 \sim 2.5\text{Mpc}$, $r_0 \sim 4.6\text{Mpc}$ and $r_0 \sim 5.7\text{Mpc}$, corresponding to $M_h \sim 3 \times 10^{10} M_{\odot}$, $M_h \sim 2 \times 10^{11} M_{\odot}$ and $M_h \sim 5 \times 10^{11} M_{\odot}$ at $z = 3.1$, $z = 4.5$ and $z = 5.7$, respectively (Gawiser et al. 2007; Kovač et al. 2007; Ouchi et al. 2010), and their surface density is low (for instance, 0.24beam^{-1} for the $z = 3.1$ sample and the 250 and $870\mu\text{m}$ beam), meaning that any boosting to the stacked fluxes from clustering is

expected to be small.

4. RESULTS AND DISCUSSION

4.1. The far-infrared SEDs of LAEs

In Figure 3 we show the 1σ far-infrared flux limits derived from the stacking in Section 3.1, compared to Chary & Elbaz (2001) SED templates and spirals and starburst galaxies in the SWIRE compilation (Polletta et al. 2007). The templates are all scaled to the $870\mu\text{m}$ flux density limits, and for the $z = 4.5$ sample none violate the 250 , 350 or $500\mu\text{m}$ limits. For the $z = 2.8$ and $z = 3.1$ galaxies the warmest SEDs violate the 1σ 250 and $350\mu\text{m}$ flux limits, although none are excluded at the $\geq 3\sigma$ level. The $z = 2.8$ LAEs are detected at 1.7 , 1.8 , and 2.6σ significance at 250 , 350 and $870\mu\text{m}$, respectively, in the stacks. Taking these fluxes and their associated errors disfavours both the warmest and the coolest SEDs, including the Sd galaxy template. We conclude that LAEs at $z \sim 3$ may not be dominated by the warmest or the coolest dust SEDs, but we cannot constrain the shape of the LAE’s far-infrared SEDs beyond reasonable templates with the current data.

It has been suggested that LAEs have dust properties similar to local Sd galaxies with cooler dust emission than average (Finkelstein et al. 2009c), and thus the SWIRE Sd template is highlighted in Figure 3. However, recent measurements indicate the LAEs are typically 1 – 1.2kpc in size (Malhotra et al. 2012), which using the local correlation between star-formation intensity and dust temperature (Lehnert & Heckman 1996), suggests that LAEs may contain warmer dust (rest-frame $S_{60}/S_{100} \sim 1$) than Sd galaxies. The M82 template in

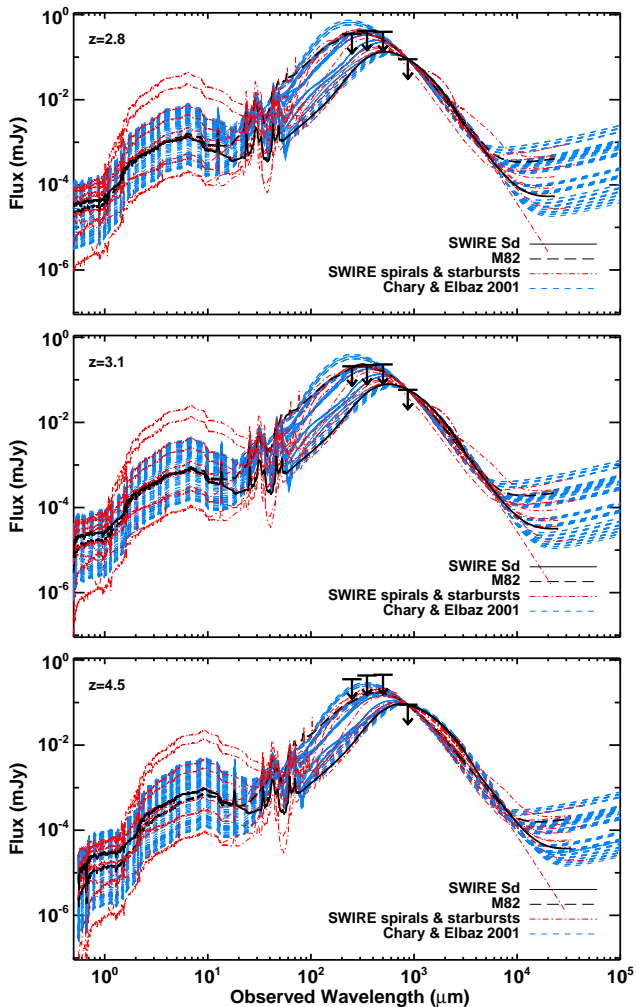


Figure 3. Observed 250, 350, 500 and $870\ \mu\text{m}$ 1σ stacked flux density limits for $z = 2.8, 3.1$ and 4.5 (top to bottom) LAEs, compared to the SEDs of starburst and late-type galaxies from the SWIRE library (Polletta et al. 2007) and Chary & Elbaz (2001) templates. The SEDs are scaled to the 1σ flux density limit at $870\ \mu\text{m}$ and we highlight the Sd and M82 templates for the reasons described Section 4.1. At $z = 4.5$ all templates are consistent with the observed limits. At $z = 2.8$ and $z = 3.1$ the 250 and $350\ \mu\text{m}$ 1σ detection limits marginally disfavour the warmest SEDs, although none are excluded at the $\geq 3\sigma$ level, and only a handful at 2σ .

the SWIRE library has $S_{60}/S_{100} \sim 1$ and therefore M82 is also highlighted in Figure 3. The hypothesis that LAEs contain warmer dust than previously anticipated is consistent with recent evidence that LAEs have lower metallicities and higher ionization parameters than LBGs of the same mass (Finkelstein et al. 2011c; McLinden et al. 2011; Nakajima et al. 2013; Richardson et al. 2013, Song et al. in prep.).

Due to the uncertainty in the shape of the typical LAE far-infrared SED we calculate the 1σ upper limit on the far-infrared ($8\text{--}1000\ \mu\text{m}$) luminosity using both the Sd and M82 templates, as well as the average luminosity, and the range of luminosities from all the templates in Figure 3. These values are listed in Table 1 and further illustrate that for a significant majority of the templates the $870\ \mu\text{m}$ limit is the most constraining of the four wavebands examined. In Table 1 we also list the 1σ limits on the SFRs, calculated from the far-infrared luminosi-

ties of the four wavelengths and four SED types, using Kennicutt (1998), which assumes a Salpeter initial mass function (IMF); divide these values by a factor of 1.7 to convert to a Chabrier (2003) IMF. We do not adjust the SFRs for potential AGN contribution to the far-infrared emission, because the AGN fraction in LAEs is small (e.g. Malhotra et al. 2003; Wang et al. 2004; Gawiser et al. 2007), although the fraction rises in the lower redshift $z \sim 2$ (Nilsson et al. 2009) and $z \sim 0.3$ (Finkelstein et al. 2009b; Cowie et al. 2009; Scarlata et al. 2009) populations. Furthermore, any adjustment for potential AGN contamination to the far-infrared fluxes would decrease the stacked flux density limits, and thus not adjusting these values is the conservative approach.

The Sd template is cooler than the majority of the SEDs, and M82 is warmer than most of the SEDs. Therefore, using the Sd template and the $870\ \mu\text{m}$ limit provides lower constraints on the far-infrared luminosity and the SFR than the M82 template (see also Figure 3). The mean of all the SEDs lies between the values provided by these two templates, and thus by considering the Sd, M82 and mean limits we bracket a wide range of possible LAE far-infrared SFRs. At $z = 2.8$ we measure 1σ SFR upper limits of 4, 23 and $15\ M_{\odot}\ \text{yr}^{-1}$ for the Sd, M82 and mean SEDs, respectively. For the $z = 3.1$ LAEs the values are 3, 15 and $9\ M_{\odot}\ \text{yr}^{-1}$, and at $z = 4.5$ we measure limits of 6, 22 and $14\ M_{\odot}\ \text{yr}^{-1}$, respectively. We note that our results for the $z = 4.5$ LAEs are consistent with Davies et al. (2013) who, for the same sample, calculated $\text{SFR} < 31\ M_{\odot}\ \text{yr}^{-1}$ (1σ), although they only considered the $870\ \mu\text{m}$ data and assumed a modified blackbody far-infrared SED with $T_D = 35\ \text{K}$ and $\beta = 2.0$.

4.2. Ly α Escape Fraction

The luminosity of the Ly α line ($L_{\text{Ly}\alpha}$) can be used to calculate a Ly α -derived star-formation rate, $\text{SFR}_{\text{Ly}\alpha}$, as

$$\text{SFR}_{\text{Ly}\alpha} (M_{\odot}\ \text{yr}^{-1}) = 9.1 \times 10^{-43} L_{\text{Ly}\alpha} (\text{erg}\ \text{s}^{-1}) \quad (1)$$

for a Salpeter IMF (Kennicutt 1998; Hu et al. 1998). The total star-formation rate is given by the sum of the unobscured and the dust-obscured (i.e. far-infrared derived) star-formation rates. The Ly α line is affected by both dust obscuration and resonant scattering by neutral hydrogen so we use the apparent (i.e. dust-uncorrected) UV luminosity to trace the unobscured SFR (SFR_{UV}). Since the intrinsic Ly α luminosity is also driven by the total star-formation rate these values can be used to calculate the Ly α escape fraction ($f_{\text{esc}}(\text{Ly}\alpha)$) as

$$f_{\text{esc}}(\text{Ly}\alpha) = \text{SFR}_{\text{Ly}\alpha} / (\text{SFR}_{\text{UV}} + \text{SFR}_{\text{FIR}}), \quad (2)$$

where SFR_{FIR} is the far-infrared derived (i.e. obscured) SFR for a Salpeter IMF²⁵.

For the LAEs in our sample the Ly α luminosity, and hence $\text{SFR}_{\text{Ly}\alpha}$, is derived either from flux-calibrated spectroscopy (e.g. Zheng et al. 2013) or from the magnitudes of the systems in narrowband compared to continuum imaging (e.g. Gronwall et al. 2007; Ciardullo et al. 2012). For the $z = 2.8, 3.1$ and 4.5 LAEs in our analyses the average $\text{SFR}_{\text{Ly}\alpha} = 2.5, 1.5$ and $7.0\ M_{\odot}\ \text{yr}^{-1}$, respectively, and the values for SFR_{UV} are 6.0, 1.9 and

²⁵ For a top-heavy IMF the ratio of ionizing to non-ionizing photons will be higher, which will preferentially increase the derived $\text{SFR}_{\text{Ly}\alpha}$ (e.g. Finkelstein et al. 2011a) and observed $f_{\text{esc}}(\text{Ly}\alpha)$.

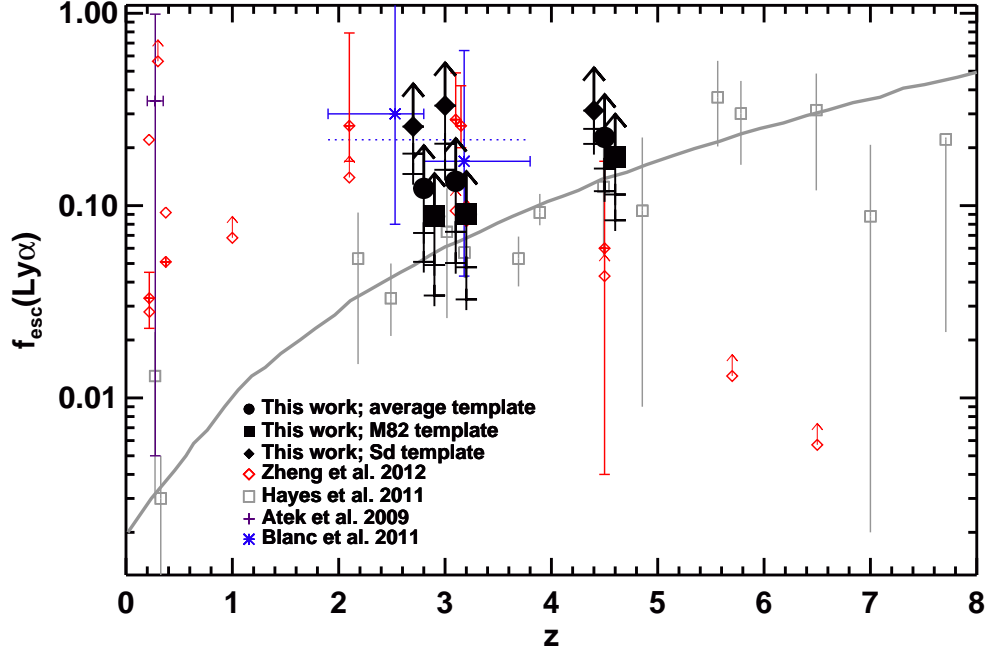


Figure 4. The Ly α escape fraction of LAEs as a function of redshift. The large symbols are our 1σ limits derived for three different SED templates from the $870\text{-}\mu\text{m}$ stacking of LAEs (with the result for the Sd and M82 templates offset slightly in z for clarity); the 2σ and 3σ limits are shown by the lines and tickmarks below each symbol. We compare with X-ray stacking results (Zheng et al. 2012) and spectroscopic and optical photometric measurements (Atek et al. 2009; Blanc et al. 2011). The grey points and line show the redshift evolution of the *global* Ly α escape fraction (Hayes et al. 2011). At all redshifts the LAE Ly α escape fractions that we measure using far-infrared emission and the average template or that of M82, are consistent with the global evolution at the $\sim 2\text{--}3\sigma$ level. However, the result using the Sd galaxy templates points to a higher Ly α escape fraction for LAEs than is globally observed.

$17M_{\odot}\text{yr}^{-1}$, respectively. SFR_{UV} is calculated using Kennicutt (1998) and rest-frame UV luminosities from the observed broadband emission minus the effect of the Ly α line (e.g. Ciardullo et al. 2012; Zheng et al. 2014). Since the UV continuum emission is derived from broadband data we also apply a correction for attenuation by the intergalactic medium (IGM) of factors of 1.29, 1.17 and 1.63 to the SFR_{UV} at $z = 2.8$, 3.1 and 4.5, respectively. The IGM correction factors are calculated using Madau (1995) and the transmission curves of the observed frame B ($z = 2.8$ sample), V and B ($z = 3.1$ sample), and R ($z = 4.5$ sample) filters. We use equation 2, the above values for $\text{SFR}_{\text{Ly}\alpha}$ and SFR_{UV} , and our measurement of the upper limit on the far-infrared (i.e. dust obscured) star-formation rates, SFR_{FIR} , to calculate lower limits on the Ly α escape fraction (Table 1). Note that the corrections for the IGM attenuation of the UV light does not affect our conclusions because equation 2 is dominated by our limits on SFR_{FIR} . As FIR measurements get deeper (e.g. with ALMA) the IGM attenuation will become more important in interpreting studies such as this.

The $870\text{-}\mu\text{m}$ data provide the tightest limits of $f_{\text{esc}}(\text{Ly}\alpha)$ and the 1σ limits from these data are shown in Figure 4 and compared with measurements of $f_{\text{esc}}(\text{Ly}\alpha)$ from LAEs at $z = 0\text{--}8$ made using optical spectroscopy and photometry (Atek et al. 2009; Blanc et al. 2011) and X-ray stacking (Zheng et al. 2012). We also compare with the global evolution of $f_{\text{esc}}(\text{Ly}\alpha)$ measured by Hayes et al. (2011).

The limits on $f_{\text{esc}}(\text{Ly}\alpha)$ at $z = 2.8$, 3.1 and 4.5, calcu-

lated using a Sd galaxy template, are all $> 3\sigma$ away from the Hayes et al. (2011) global, optically-derived measurement. This is an indication that either LAEs have a higher Ly α $f_{\text{esc}}(\text{Ly}\alpha)$ than globally observed, or that they contain warmer dust than typical local Sd galaxies. For the LAEs in all the redshift bins our far-infrared determinations of $f_{\text{esc}}(\text{Ly}\alpha)$ using the M82 template are consistent, at the $1\text{--}2\sigma$ level, with the X-ray results (Zheng et al. 2012) and the optical determination of the global $f_{\text{esc}}(\text{Ly}\alpha)$ from Hayes et al. (2011). For the $z = 2.8$ and $z = 4.5$ LAEs the 3σ limit on the $f_{\text{esc}}(\text{Ly}\alpha)$ measured using the average far-infrared SED is at the threshold of being consistent with the global evolution.

If we consider the 2.6σ significance detection of the stacked $z = 2.8$ LAEs at $870\text{-}\mu\text{m}$ (Section 3.1) as real, then the inferred $\text{SFR}_{\text{FIR}} = 10 \pm 4M_{\odot}\text{yr}^{-1}$, $58 \pm 23M_{\odot}\text{yr}^{-1}$, $37 \pm 15M_{\odot}\text{yr}^{-1}$ (where the errors represent the $870\text{-}\mu\text{m}$ photometric uncertainty) for the Sd, M82 and average of the SEDs, respectively. In this case the inferred $f_{\text{esc}}(\text{Ly}\alpha)$ are 0.16 ± 0.04 , 0.04 ± 0.01 , and 0.08 ± 0.02 , respectively. For the M82 and average SED these values are consistent with the global $f_{\text{esc}}(\text{Ly}\alpha)$, but for the Sd galaxy template the inferred LAE $f_{\text{esc}}(\text{Ly}\alpha)$ is significantly higher than the global $f_{\text{esc}}(\text{Ly}\alpha)$ evolution (Hayes et al. 2011). Note also, that the $1\text{--}2\sigma$ significance detections of the $z = 2.8$ stacks at 250 and $350\text{-}\mu\text{m}$ disfavour the Sd SED (see Section 3.1).

4.3. Comparison with previous results

Oteo et al. (2012) cross-matched 56 UV-bright $z = 2\text{--}3.5$ LAEs with *Herschel*-PACS 70, 100 and $160\text{-}\mu\text{m}$ cat-

alogs. Of their 56 LAEs four were detected at $160\ \mu\text{m}$ (3σ ; $S_{160} \geq 2.0\ \text{mJy}$), indicating $L_{\text{IR}} \geq 10^{12} L_{\odot}$ for Chary & Elbaz (2001) SEDs – significantly brighter than the averages of our samples. However, Oteo et al. (2012) did not perform far-infrared analyses (such as stacking) of their individually-undetected population and therefore, it is unclear whether the apparent difference between the samples is due to the UV-bright nature of their LAEs, cosmic variance, the assumed SEDs, or potentially mis-matching between the PACS source and the LAEs.

At higher redshift, Ouchi et al. (2013) recently failed to detect both 1.2 mm continuum and the [C II] $158\ \mu\text{m}$ emission line from the extended $z = 6.6$ LAE ‘Himiko’ with ALMA. Using their limit on L_{IR} yields $f_{\text{esc}}(\text{Ly}\alpha) > 0.80$ (1σ) – significantly higher than expected from the global evolution (Hayes et al. 2011, see also Figure 4), although as Himiko is spatially extended the relevant physical effects may be different. We also caution that at $z = 6.6$ the CMB temperature ($\sim 20\ \text{K}$) can make it harder to detect a galaxy’s dust emission (e.g. da Cunha et al. 2013), an effect that Ouchi et al. (2013) did not explicitly include in their calculations, and which could increase the far-infrared luminosity limit and decrease the $f_{\text{esc}}(\text{Ly}\alpha)$ limit. However, the high $f_{\text{esc}}(\text{Ly}\alpha)$ is consistent with the hypothesis that Himiko has low metallicity and low dust content (Ouchi et al. 2013).

Another $z \sim 6$ system – HFLS3 was identified on the basis of its bright dust emission and does not have a similar metallicity and dust deficit (Riechers et al. 2013). The $\text{Ly}\alpha$ line was not detected in LRIS spectroscopy but it is in a region of significant skyline contamination. At $z = 4.76$ LESS J033229 was also identified on the basis of bright dust emission, but it is detected in $\text{Ly}\alpha$ (Coppin et al. 2009) with $\text{SFR}_{\text{Ly}\alpha} = 4\ \text{M}_{\odot}\text{yr}^{-1}$, compared to $\text{SFR}_{\text{FIR}} \sim 1000\ \text{M}_{\odot}\text{yr}^{-1}$ (Swinbank et al. 2013) – indicating $f_{\text{esc}}(\text{Ly}\alpha) \sim 0.003$. The apparent difference between the $f_{\text{esc}}(\text{Ly}\alpha)$ measured for high-redshift submillimeter galaxies and LAEs is likely a selection effect – submillimeter galaxies are selected on the basis of their dust emission and extreme star-formation rates, whereas LAEs are identified via the (unobscured) $\text{Ly}\alpha$ emission.

4.4. Future Prospects

Having used the deepest available data to probe the far-infrared SEDs of $z = 2.8, 3.1$ and 4.5 LAEs we can place tight limits on the required depths for future surveys that aim to detect LAEs at far-infrared wavelengths. Using higher resolution observations, which have lower confusion limits and can provide deeper data (e.g. the 450 and $850\ \mu\text{m}$ SCUBA-2 Cosmology Legacy Survey²⁶), or stacking on a larger number of LAEs is required. Alternatively, interferometric observations targeting individual sources can be used as their small resolutions can probe below the confusion limit of single-dish surveys.

At $\sim 870\ \mu\text{m}$ surveys aiming to detect individual LAEs will need to probe below our observed 1σ limits of 0.09, 0.06 and $0.09\ \text{mJy beam}^{-1}$ at $z = 2.8, 3.1$ and 4.5 , respectively. For example, continuum mapping with ALMA could reach $0.05\ \text{mJy rms}$ (\sim twice as deep as our stacks) in band 7 ($850\ \mu\text{m}$) in just 15 minutes of integration per source. It is clear from Figure 3 that data shorter

than the far-infrared peak at rest-frame $\sim 60\text{--}100\ \mu\text{m}$ are also required to properly characterize the SEDs and derive accurate measurements of the far-infrared luminosities, SFRs and hence the $\text{Ly}\alpha$ escape fraction of LAEs. Ground-based observations are more challenging at these wavelengths – for instance, ALMA will take 1.5 hours per source to reach $0.2\ \text{mJy beam}^{-1}$ in band 9 ($500\ \mu\text{m}$) – meaning that stacking will still be an attractive prospect to constrain the shape of the SEDs.

5. CONCLUSIONS

We have examined the far-infrared SEDs of 126, 280 and 92 LAEs in the ECDFS at redshifts 2.8, 3.1 and 4.5, respectively. None of the LAEs are reliably individually detected in *Herschel* (HerMES) imaging at 250, 350 or $500\ \mu\text{m}$, or in LABOCA (LESS) data at $870\ \mu\text{m}$.

Therefore, we stacked data at the positions of the LAEs in each redshift slice to probe deeper into their average far-infrared emission, reaching $1\sigma = 0.09, 0.06$ and $0.09\ \text{mJy}$ at $870\ \mu\text{m}$ for the $z = 2.8, 3.1$ and 4.5 LAEs. The average emission was not detected at $\geq 3\sigma$ in any of the stacks and we find that the $870\ \mu\text{m}$ flux limits provide the deepest constraints on the LAEs far-infrared luminosities. We use the 4-band photometric limits to examine the shape of the LAEs’ SEDs, and although the warmest SEDs are marginally disfavoured the shorter wavelength data are not deep enough to confidently exclude any.

We calculate upper limits on the far-infrared emission from LAEs at each redshift using M82, an Sd galaxy and our average galaxy SED templates. The LAEs have $L_{\text{IR}} \lesssim 10^{11} L_{\odot}$, although the values vary for the different redshift slices and SED shapes considered (see Table 1). The luminosity limits were then used to calculate upper limits on dust-obscured SFRs of LAEs of a few to a few tens $\text{M}_{\odot}\text{yr}^{-1}$ on average.

Since the far-infrared SFR probes dust-obscured star-formation, and UV emission probes unobscured star-formation they can be combined to calculate the total SFR in the LAEs. This total SFR traces the intrinsic $\text{Ly}\alpha$ luminosity, and we use it to calculate lower limits on the $\text{Ly}\alpha$ escape fraction for LAEs at $z = 2.8, 3.1$ and 4.5 . We find escape fractions of $\gtrsim 10\%$ (1σ) at all the redshifts considered, although the exact values vary with redshift and the SED used to calculate the far-infrared luminosity. These limits are broadly consistent with the global evolution of $f_{\text{esc}}(\text{Ly}\alpha)$ at the $\sim 1\text{--}3\sigma$ level, with the exception of the results derived for the Sd galaxy SED template, where the escape fractions are $> 30\%$ in all cases.

We thank Ian Smail and Fabian Walter for helpful discussions and feedback on this manuscript. JLW, AC and DR thank the Aspen Center for Physics for hospitality during the conception, writing and editing of this paper. This work is supported in part by the NSF under Grant Numbers PHY-1066293 and AST-1055919. SM and JR thank the DARK Cosmology Centre and Nordea Fonden in Copenhagen, Denmark, for hospitality during the course of this work. The Dark Cosmology Centre is funded by the Danish National Research Foundation. We acknowledge support from the Science and Technology Facilities Council [grant number ST/I000976/1].

²⁶ www.jach.hawaii.edu/JCMT/surveys/Cosmology.html

Based on observations collected at the European Organisation for Astronomical Research in the Southern Hemisphere, Chile, under programmes 078.F-9028(A), 079.F-9500(A), 080.A-3023(A), and 081.F-9500(A). This research has made use of data from the HerMES project ([\protecthttp://hermes.sussex.ac.uk](http://hermes.sussex.ac.uk)). HerMES is a Herschel Key Programme utilizing Guaranteed Time from the SPIRE instrument team, ESAC scientists and a mission scientist. HerMES is described in Oliver et al. (2012). The data presented in this paper will be released through the HerMES Database in Marseille, HeDaM (<http://hedam.oamp.fr/HerMES>) SPIRE has been developed by a consortium of institutes led by Cardiff Univ. (UK) and including: Univ. Lethbridge (Canada); NAOC (China); CEA, LAM (France); IFSI, Univ. Padua (Italy); IAC (Spain); Stockholm Observatory (Sweden); Imperial College London, RAL, UCL-MSSL, UKATC, Univ. Sussex (UK); and Caltech, JPL, NHSC, Univ. Colorado (USA). This development has been supported by national funding agencies: CSA (Canada); NAOC (China); CEA, CNES, CNRS (France); ASI (Italy); MCINN (Spain); SNSB (Sweden); STFC, UKSA (UK); and NASA (USA).

Facilities: APEX (LABOCA), Herschel (SPIRE)

REFERENCES

- Atek, H., Kunth, D., Schaerer, D., Hayes, M., Deharveng, J. M., Östlin, G., & Mas-Hesse, J. M. 2009, *A&A*, 506, L1
 Baker, J. G., & Menzel, D. H. 1938, *ApJ*, 88, 52
 Béthermin, M., Dole, H., Beelen, A., & Aussel, H. 2010, *A&A*, 512, A78
 Biggs, A. D., et al. 2011, *MNRAS*, 413, 2314
 Blanc, G. A., et al. 2011, *ApJ*, 736, 31
 Calanog, J. A., et al. 2013, *ApJ*, 775, 61
 Calzetti, D., et al. 2010, *ApJ*, 714, 1256
 Chabrier, G. 2003, *PASP*, 115, 763
 Chapman, S. C., Blain, A. W., Smail, I., & Ivison, R. J. 2005, *ApJ*, 622, 772
 Chary, R., & Elbaz, D. 2001, *ApJ*, 556, 562
 Choi, P. I., et al. 2006, *ApJ*, 637, 227
 Ciardullo, R., et al. 2012, *ApJ*, 744, 110
 Coppin, K. E. K., et al. 2009, *MNRAS*, 395, 1905
 Cowie, L. L., Barger, A. J., & Hu, E. M. 2010, *ApJ*, 711, 928
 Cowie, L. L., Barger, A. J., Wang, W.-H., & Williams, J. P. 2009, *ApJ*, 697, L122
 Cowie, L. L., & Hu, E. M. 1998, *AJ*, 115, 1319
 da Cunha, E., et al. 2013, *ApJ*, 766, 13
 Davies, L. J. M., Bremer, M. N., Stanway, E. R., & Lehnert, M. D. 2013, *MNRAS*, 433, 2588
 Dawson, S., Rhoads, J. E., Malhotra, S., Stern, D., Wang, J., Dey, A., Spinrad, H., & Jannuzi, B. T. 2007, *ApJ*, 671, 1227
 Deharveng, J.-M., et al. 2008, *ApJ*, 680, 1072
 Egami, E., et al. 2004, *ApJS*, 154, 130
 Fernandez-Conde, N., Lagache, G., Puget, J.-L., & Dole, H. 2010, *A&A*, 515, A48
 Finkelstein, K. D., et al. 2011a, *ApJ*, 742, 108
 Finkelstein, S. L., Cohen, S. H., Malhotra, S., & Rhoads, J. E. 2009a, *ApJ*, 700, 276
 Finkelstein, S. L., Cohen, S. H., Malhotra, S., Rhoads, J. E., Papovich, C., Zheng, Z. Y., & Wang, J.-X. 2009b, *ApJ*, 703, L162
 Finkelstein, S. L., Cohen, S. H., Moustakas, J., Malhotra, S., Rhoads, J. E., & Papovich, C. 2011b, *ApJ*, 733, 117
 Finkelstein, S. L., Malhotra, S., Rhoads, J. E., Hathi, N. P., & Pirzkal, N. 2009c, *MNRAS*, 393, 1174
 Finkelstein, S. L., Rhoads, J. E., Malhotra, S., & Grogin, N. 2009d, *ApJ*, 691, 465
 Finkelstein, S. L., Rhoads, J. E., Malhotra, S., Grogin, N., & Wang, J. 2008, *ApJ*, 678, 655
 Finkelstein, S. L., et al. 2011c, *ApJ*, 729, 140
 Gawiser, E., et al. 2006, *ApJS*, 162, 1
 —. 2007, *ApJ*, 671, 278
 Greve, T. R., et al. 2010, *ApJ*, 719, 483
 Griffin, M. J., et al. 2010, *A&A*, 518, L3
 Grimm, H.-J., Gilfanov, M., & Sunyaev, R. 2003, *MNRAS*, 339, 793
 Gronwall, C., et al. 2007, *ApJ*, 667, 79
 Guaita, L., et al. 2010, *ApJ*, 714, 255
 Hansen, M., & Oh, S. P. 2006, *MNRAS*, 367, 979
 Hayes, M., Schaerer, D., Östlin, G., Mas-Hesse, J. M., Atek, H., & Kunth, D. 2011, *ApJ*, 730, 8
 Hayes, M., et al. 2010, *Nature*, 464, 562
 Heinis, S., et al. 2013, *MNRAS*, 429, 1113
 Hodge, J. A., et al. 2013, *ApJ*, 768, 91
 Hu, E. M., Cowie, L. L., Capak, P., McMahon, R. G., Hayashino, T., & Komiyama, Y. 2004, *AJ*, 127, 563
 Hu, E. M., Cowie, L. L., & McMahon, R. G. 1998, *ApJ*, 502, L99
 Ivison, R. J., Smail, I., Le Borgne, J., Blain, A. W., Kneib, J., Bezecourt, J., Kerr, T. H., & Davies, J. K. 1998, *MNRAS*, 298, 583
 Ivison, R. J., et al. 2007, *MNRAS*, 380, 199
 —. 2010, *MNRAS*, 402, 245
 Iye, M., et al. 2006, *Nature*, 443, 186
 Kennicutt, Jr., R. C. 1998, *ARA&A*, 36, 189
 Kovač, K., Somerville, R. S., Rhoads, J. E., Malhotra, S., & Wang, J. 2007, *ApJ*, 668, 15
 Kurczynski, P., & Gawiser, E. 2010, *AJ*, 139, 1592
 Lehnert, M. D., & Heckman, T. M. 1996, *ApJ*, 472, 546
 Levenson, L., et al. 2010, *MNRAS*, 409, 83
 Madau, P. 1995, *ApJ*, 441, 18
 Malhotra, S., Rhoads, J. E., Finkelstein, S. L., Hathi, N., Nilsson, K., McLinden, E., & Pirzkal, N. 2012, *ApJ*, 750, L36
 Malhotra, S., Wang, J. X., Rhoads, J. E., Heckman, T. M., & Norman, C. A. 2003, *ApJ*, 585, L25
 Marsden, G., et al. 2009, *ApJ*, 707, 1729
 McLinden, E. M., et al. 2011, *ApJ*, 730, 136
 Murphy, E. J., et al. 2011, *ApJ*, 737, 67
 Nakajima, K., Ouchi, M., Shimasaku, K., Hashimoto, T., Ono, Y., & Lee, J. C. 2013, *ApJ*, 769, 3
 Nandra, K., Mushotzky, R. F., Arnaud, K., Steidel, C. C., Adelberger, K. L., Gardner, J. P., Teplitz, H. L., & Windhorst, R. A. 2002, *ApJ*, 576, 625
 Neufeld, D. A. 1991, *ApJ*, 370, L85
 Nilsson, K. K., Tapken, C., Möller, P., Freudling, W., Fynbo, J. P. U., Meisenheimer, K., Laursen, P., & Östlin, G. 2009, *A&A*, 498, 13
 Nonino, M., et al. 2009, *ApJS*, 183, 244
 Oliver, S. J., et al. 2012, *MNRAS*, 424, 1614
 Oteo, I., et al. 2012, *A&A*, 541, A65
 Ouchi, M., et al. 2008, *ApJS*, 176, 301
 —. 2009, *ApJ*, 706, 1136
 —. 2010, *ApJ*, 723, 869
 —. 2013, *arXiv:1306.3572*
 Partridge, R. B., & Peebles, P. J. E. 1967, *ApJ*, 147, 868
 Pascale, E., et al. 2009, *ApJ*, 707, 1740
 Peacock, J. A., et al. 2000, *MNRAS*, 318, 535
 Penner, K., et al. 2011, *MNRAS*, 410, 2749
 Persic, M., Rephaeli, Y., Braito, V., Cappi, M., Della Ceca, R., Franceschini, A., & Gruber, D. E. 2004, *A&A*, 419, 849
 Pilbratt, G. L., et al. 2010, *A&A*, 518, L1
 Polletta, M., et al. 2007, *ApJ*, 663, 81
 Ranalli, P., Comastri, A., & Setti, G. 2003, *A&A*, 399, 39
 Rhoads, J. E., Hibon, P., Malhotra, S., Cooper, M., & Weiner, B. 2012, *ApJ*, 752, L28
 Rhoads, J. E., Malhotra, S., Dey, A., Stern, D., Spinrad, H., & Jannuzi, B. T. 2000, *ApJ*, 545, L85
 Rhoads, J. E., et al. 2003, *AJ*, 125, 1006
 Richardson, M. L. A., Levesque, E. M., McLinden, E. M., Malhotra, S., Rhoads, J. E., & Xia, L. 2013, *arXiv:1309.1169*
 Riechers, D. A., et al. 2013, *Nature*, 496, 329
 Rieke, G. H., Alonso-Herrero, A., Weiner, B. J., Pérez-González, P. G., Blaylock, M., Donley, J. L., & Marcillac, D. 2009, *ApJ*, 692, 556
 Scarlata, C., et al. 2009, *ApJ*, 704, L98
 Serjeant, S., et al. 2004, *ApJS*, 154, 118
 —. 2008, *MNRAS*, 386, 1907
 —. 2010, *A&A*, 514, A10+
 Shibuya, T., Kashikawa, N., Ota, K., Iye, M., Ouchi, M., Furusawa, H., Shimasaku, K., & Hattori, T. 2012, *ApJ*, 752, 114
 Smith, A. J., et al. 2012, *MNRAS*, 419, 377
 Steidel, C. C., Adelberger, K. L., Giavalisco, M., Dickinson, M., & Pettini, M. 1999, *ApJ*, 519, 1
 Symeonidis, M., et al. 2011, *MNRAS*, 417, 2239
 Viero, M. P., et al. 2012, *MNRAS*, 421, 2161
 —. 2013a, *ApJ*, 772, 77
 —. 2013b, *arXiv:1304.0446*
 Wang, J.-X., Malhotra, S., Rhoads, J. E., Zhang, H.-T., & Finkelstein, S. L. 2009, *ApJ*, 706, 762
 Wang, J. X., et al. 2004, *ApJ*, 608, L21
 Weiß, A., et al. 2009, *ApJ*, 707, 1201
 Zheng, Z.-Y., Wang, J.-X., Malhotra, S., Rhoads, J. E., Finkelstein, S. L., & Finkelstein, K. 2014, *MNRAS*, 439, 1101

Zheng, Z.-Y., et al. 2012, *ApJ*, 746, 28
—, 2013, *MNRAS*, 431, 3589